

# **Supplementary Information**

## **Structure of human mitochondrial RNA polymerase elongation complex**

**Kathrin Schwinghammer<sup>1</sup>, Alan C.M. Cheung<sup>1</sup>, Yaroslav I. Morozov<sup>2</sup>, Karen Agaronyan<sup>2</sup>, Dmitry Temiakov<sup>2</sup> and Patrick Cramer<sup>1</sup>**

<sup>1</sup>Gene Center and Department of Biochemistry, Ludwig-Maximilians-Universität München, Munich, Germany.

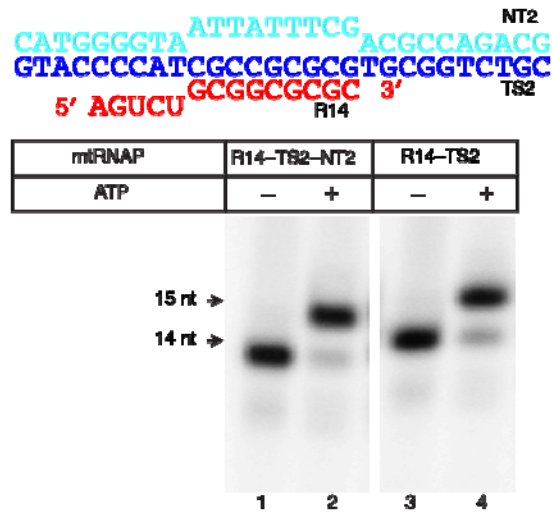
<sup>2</sup>Department of Cell Biology, School of Osteopathic Medicine, Rowan University, Stratford, New Jersey, USA.

**Supplementary Information comprises:**

**Supplementary Figures 1–5**

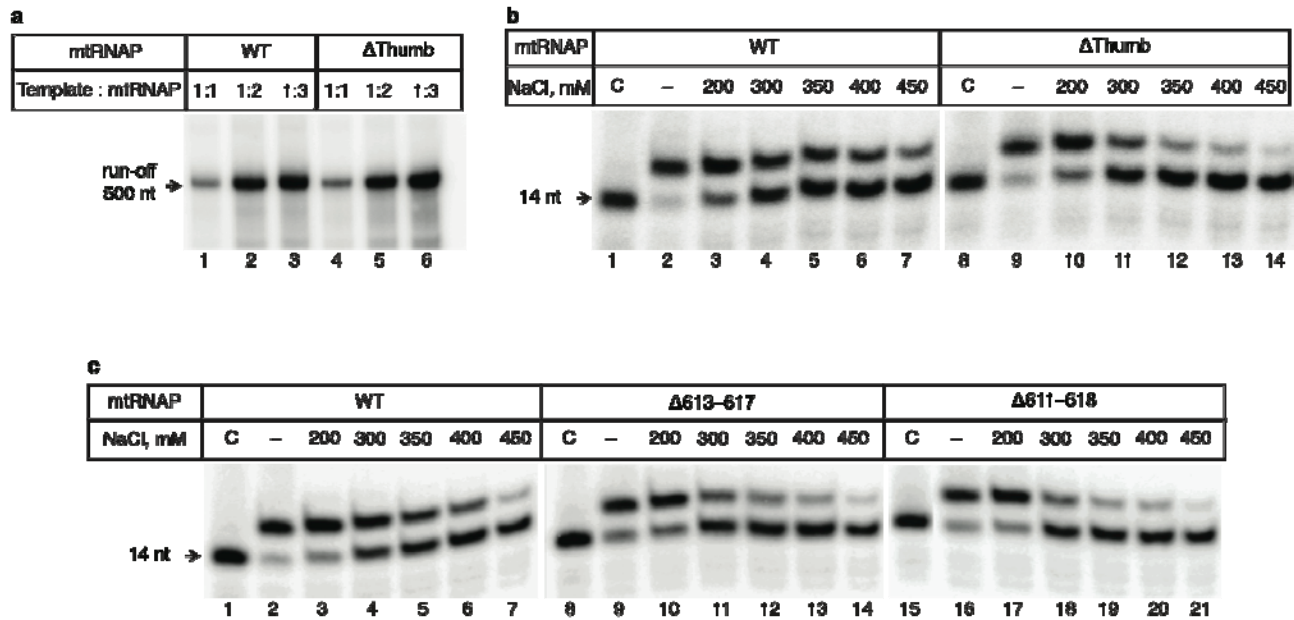
**Supplementary Tables 1–2**

**Supplementary Video 1**



**Supplementary Figure 1** Activity of mtRNAP elongation complex assembled on nucleic acid scaffolds.

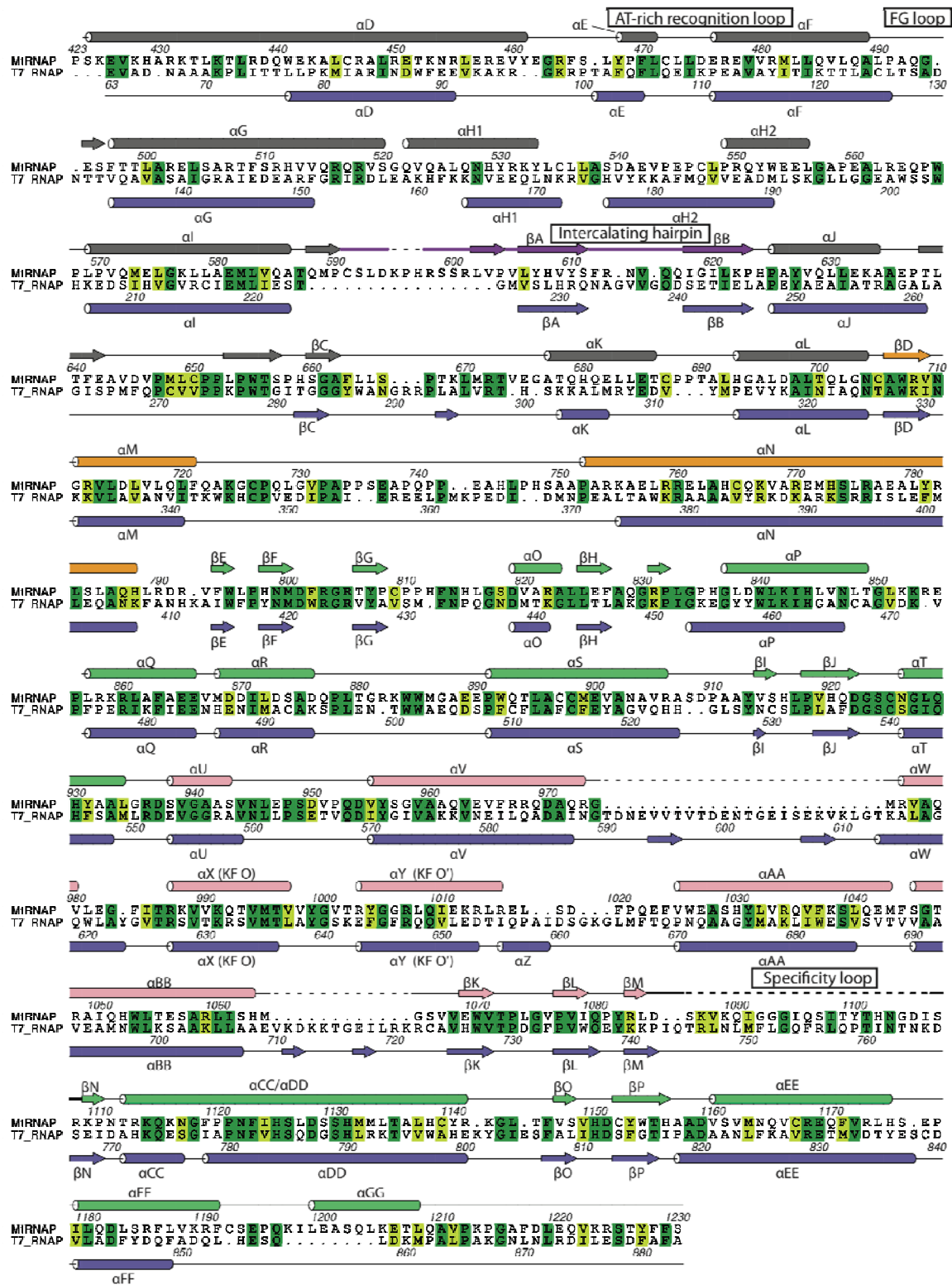
mtRNAP (1 mM) was pre-incubated with the scaffolds indicated (1 mM) for 5 min at room temperature and the  $^{32}\text{P}$ -labeled RNA primer extended by addition of 10 mM of adenosine triphosphate (ATP) for 2 min. The products of the reaction were resolved in 20% PAGE containing 6 M urea.



**Supplementary Figure 2** Effects of mtRNAP variants on elongation complex stability.

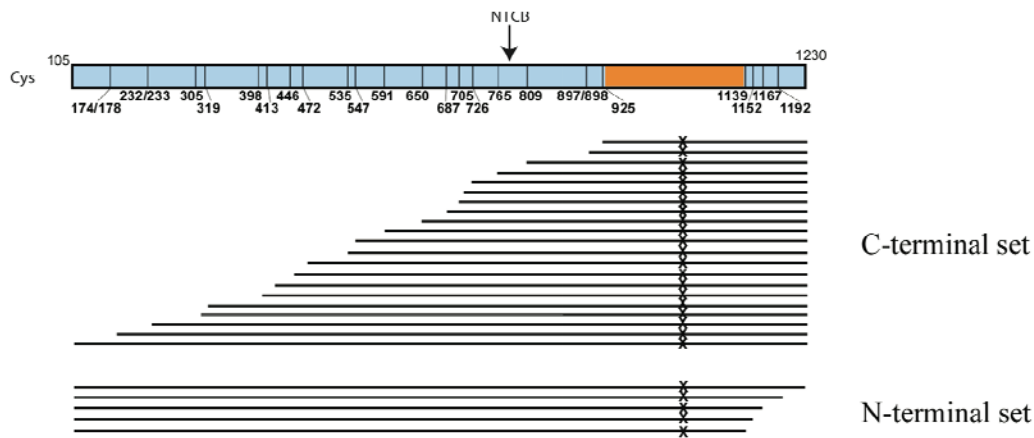
**(a,b)** Thumb deletion mtRNAP mutant is processive but forms unstable halted elongation complexes. **(a)** Processivity of the  $\Delta$ thumb mtRNAP. Run-off transcription assay was performed using PCR template containing the LSP promoter (50 nM) and the indicated amount of WT (lanes 1–3) and  $\Delta$ thumb (lanes 4–6) mtRNAPs and the products of the reactions resolved in 20% PAGE containing 6 M urea. **(b)**  $\Delta$ Thumb mutant forms an unstable halted elongation complex. The elongation complexes were assembled using R14–TS2–NT2 scaffold and WT or  $\Delta$ thumb mtRNAP. As a control (C) only polymerase was loaded in lanes 1 and 8.

**(c)** Elongation complexes formed with mtRNAP variants that contain a deletion of the intercalating hairpin are sensitive to salt challenge. Elongation complexes were formed using R14–TS2–NT2 scaffold and WT (lanes 1–7) or the intercalating hairpin deletion mutants  $\Delta$ 613–617 (lanes 8–14) and  $\Delta$ 611–618 (lanes 15–21). As a control (C) only polymerase was loaded in lanes 1,8 and 15.



Supplementary Figure 3 Structure-based sequence alignment and conservation of human mtRNAP (residues 423–1230) and T7 RNAP (residues 63–883, PDB 1QLN)<sup>1,2</sup>.

Secondary structure elements are consecutively labeled in alphabetical order (cylinders,  $\alpha$ -helices; arrows,  $\beta$ -strands; lines, loops). Since helix X is commonly named helix O based on a corresponding helix in the *Escherichia coli* Klenow (KF) fragment<sup>3</sup>, we maintain this convention during this work. Identical residues are highlighted in dark green, conservative substitutions are shown light green. Color coding for mtRNAP secondary elements is as in **Figs. 1–3**.



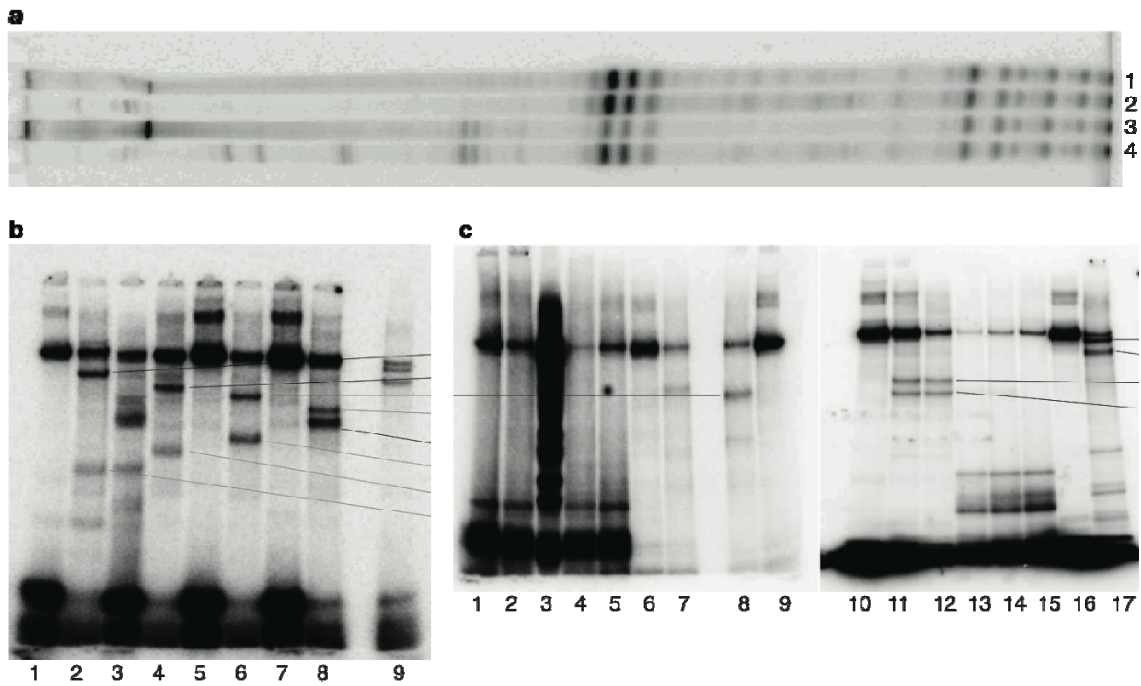
**Supplementary Figure 4** Analysis of cross-linking mapping data.

Cross-linking mapping with NTCB and CNBr (**Fig. 4a**) was performed using the so-called “single-hit” conditions<sup>4,5</sup> i.e. when every mtRNAP molecule is cleaved only once, on average. Thus, the single-hit conditions generate characteristic patterns of the N-terminal and C-terminal cleavage products. As an example, the theoretical pattern of mtRNAP cleavage by NTCB consistent with the position of the cross-link at the C-terminus is presented above. The size of the labeled fragments is identified by its mass (mobility in SDS PAGE) using SeeBlue protein standard markers (Invitrogen). To distinguish between the C-terminal and the N-terminal location of the cross-link two variants of mtRNAP were used, WT mtRNAP and  $\Delta 104$  mtRNAP (**Fig. 4a**). No shift in bands migration was observed in SDS-PAGE (**Fig. 4a**, lanes 2 and 3) confirming the location of the cross-link site at the C-terminus of mtRNAP. The smallest labeled band visible on the SDS PAGE upon NTCB treatment corresponds to the 925–1230 peptide and thus positions the cross-linking site between residues C925 and C1139. This interval was narrowed down even further by CNBr cleavage (**Fig. 4a**, lanes 5 and 6). The smallest band visible on the gel upon CNBr treatment corresponds to the 1064–1230 peptide and positions the cross-linking site between residues M1063 and M1132.

Cross-linking mapping of RNA at base –13 was performed using mtRNAP variants having a single hydroxylamin cleavage site (NG pair) at a defined position (**Fig. 4b**). The cleavage generates only two mtRNAP fragments simplifying identification of the labeled peptides. Thus the cleavage of the cross-link obtained with NG493 mutant

results in appearance of a labeled fragment (83.2 kDa) representing the C-terminus of mtRNAP, while cleavage of NG634 mutant results in appearance of the N-terminal fragment (61.5 kDa). Taken together, these data suggest that the cross-linking site is between residues 494 and 634.

Mapping of cross-link at DNA template base at -8 (**Fig. 4c**) was performed using  $\text{NH}_2\text{OH}$  and WT, NG556 and NG634 mtRNAPs. WT mtRNAP contains four sites for  $\text{NH}_2\text{OH}$  cleavage at positions 710, 926, 1103 and 1117, however the most N-terminal site (710) is cleaved inefficiently and thus the resulting peptides are not visible.  $\text{NH}_2\text{OH}$  cleavage of the mtRNAP-DNA cross-link results in two major products corresponding to the intervals 44–926 and 44–1103 or 44–1117 (**Fig. 4c**, lane 6). Since no band was observed that corresponds to the interval 926–1103 or 926–1117 (about 28 kDa for peptide with the cross-linked DNA) we conclude that the cross-link is to the 44–926 interval of mtRNAP. Cleavage of the NG556 mutant results in appearance of the labeled C-terminal fragment (around 82 kDa), while cleavage of NG634 mutant generates two labeled fragments representing both the C- and the N-terminal parts of mtRNAP (**Fig. 4c**, lanes 1–4). Taken together these data suggest that the cross-link site of -8 base of DNA includes two adjacent mtRNAP regions: 557–634 and 635–926.



**Supplementary Figure 5** Uncropped autoradiographs.

**(a)** Autoradiograph of transcription run-off assays, lanes 1–4 were used to prepare **Fig. 3d**.

**(b–c)** Autoradiograph of cross-linking experiments. **(b)** lanes 1,2,4,6,8 were used to prepare **Fig. 4b**, **(c)** lanes 16,7,10,11,16,17 were used to prepare **Fig. 4c**.



**Supplementary Table 1** Base pair parameters of mtRNAP elongation complex DNA-RNA hybrid region.

Register	Base pair	Shear (Å)	Stretch (Å)	Stagger (Å)	Buckle (°)	Propeller (°)	Opening (°)
+1	G-C	-0.57	-0.13	-0.28	-13.85	-11.09	4.34
-1	C-G	-0.12	-0.23	0.43	-2.82	-11.09	-2.26
-2	G-C	0.01	-0.22	0.14	-8.82	-9.62	-2.76
-3	G-C	-0.3	-0.13	-0.19	-9.93	-16.22	2.08
-4	C-G	0.46	-0.18	0.02	-0.39	-11.15	0.54
-5	G-C	-0.06	-0.16	-0.02	-1.93	-12.26	-1.6
-6	C-G	0.24	-0.16	0.21	-0.48	-15.32	3
-7	G-C	-0.5	-0.1	-0.28	-21.38	-11.28	2.03
-8	C-G	-0.13	-0.13	0.18	-10.77	0.16	-2.17

Register	Step	Shift (Å)	Slide (Å)	Rise (Å)	Tilt (°)	Roll (°)	Twist (°)
+1/-1	GC/GC	-0.47	-0.48	3.16	-7.74	-0.55	32.53
-1/-2	CG/CG	0.4	-1.53	3.27	4.4	6.94	33.32
-2/-3	GG/CC	0.16	-1.18	3.31	3.38	11.58	32.11
-3/-4	GC/GC	0.47	-1.14	3.08	-1.28	7.37	29.52
-4/-5	CG/CG	-0.08	-1.85	3.3	-0.65	9.86	27.91
-5/-6	GC/GC	0.24	-1.69	3.24	-1.05	4.83	29.64
-6/-7	CG/CG	0.57	-1.16	3.65	9.92	10.14	35.42
-7/-8	GC/GC	-0.15	-0.64	3.16	-2.61	13.59	28.98

**Supplementary Table 2** Structural comparison of mtRNAP elongation complex NTD with different T7 NTD complexes by C $\alpha$  root-mean-square deviation (RMSD) values. Structures were aligned based on the sequence alignment (**Supplementary Fig. 3**) and the RMSD calculated over all matching C $\alpha$  pairs.

mtRNAP elongation complex NTD (residues 426–638) superimposed with:	RMSD (Å)
T7 initiation structure (PDB 1QLN <sup>1</sup> , residues 72–261)	6.4
T7 initiation–elongation intermediate (PDB 3E2E <sup>6</sup> , residues 73–254)	4.7
T7 pre–translocated product structure (PDB 1S77 <sup>7</sup> , residues 63–261)	8.3
T7 post–translocated structure (PDB 1MSW (ref. 8), residues 63–261)	8.0

**Supplementary Video 1.** Animation of the structural rearrangements between apo mtRNAP (PDB 3SPA<sup>9</sup>) and its elongation complex.  
The movie was generated using the morphing function of UCSF Chimera<sup>10</sup>.

## Supplementary references

- 1 Cheetham, G. M. & Steitz, T. A. Structure of a transcribing T7 RNA polymerase initiation complex. *Science* **286**, 2305-2309 (1999).
- 2 Bond, C. S. & Schuttelkopf, A. W. ALINE: a WYSIWYG protein-sequence alignment editor for publication-quality alignments. *Acta Crystallogr D Biol Crystallogr* **65**, 510-512 (2009).
- 3 Beese, L. S., Derbyshire, V. & Steitz, T. A. Structure of DNA polymerase I Klenow fragment bound to duplex DNA. *Science* **260**, 352-355 (1993).
- 4 Grachev, M. A. *et al.* Studies of the functional topography of Escherichia coli RNA polymerase. A method for localization of the sites of affinity labelling. *Eur J Biochem* **180**, 577-585 (1989).
- 5 Korzheva, N. *et al.* A structural model of transcription elongation. *Science* **289**, 619-625 (2000).
- 6 Durniak, K. J., Bailey, S. & Steitz, T. A. The structure of a transcribing T7 RNA polymerase in transition from initiation to elongation. *Science* **322**, 553-557 (2008).
- 7 Yin, Y. W. & Steitz, T. A. The structural mechanism of translocation and helicase activity in T7 RNA polymerase. *Cell* **116**, 393-404 (2004).
- 8 Yin, Y. W. & Steitz, T. A. Structural basis for the transition from initiation to elongation transcription in T7 RNA polymerase. *Science* **298**, 1387-1395 (2002).
- 9 The CCP4 suite: programs for protein crystallography. *Acta Crystallogr D Biol Crystallogr* **50**, 760-763 (1994).
- 10 Yang, Z. *et al.* UCSF Chimera, MODELLER, and IMP: an integrated modeling system. *J Struct Biol* **179**, 269-278 (2012).